PERGAMON

International Journal of Multiphase Flow 28 (2002) 805–822

International Journal of Multiphase Flow

www.elsevier.com/locate/ijmulflow

The effects of mesoscale structures on the macroscopic momentum equations for two-phase flows

Duan Z. Zhang *, W. Brian VanderHeyden

Los Alamos National Laboratory Theoretical Division, Fluid Dynamics Group T-3, MS B216, Los Alamos, NM 87545, USA

Received 16 January 2001; received in revised form 16 December 2001

Abstract

Mesoscale structures (bubbles, clusters and streamers) in two-phase flows, especially in gas–solid fluidized beds significantly affect macroscopic hydrodynamic behavior. For industrial-scale fluidized beds, it is typically impractical to simulate these structures directly due to the excessive resolution required. To model effects of mesoscale structures, the ensemble phase averaging method is extended to derive macroscopic averaged equations and their closures. It is found that added-mass and drag reduction effects due to mesoscale structures play essential roles in the macroscopic equations of motion. Unlike the classical added-mass force, which is proportional to the continuous fluid density, the mesoscale added-mass force is proportional to the mixture density. Thus for gas–solid systems wherein the classical added-mass force is almost always negligible, the mesoscale added-mass force is, in contrast, found to be quite important. Mesoscale drag reduction results from the fact that, in a particle rich region, there is significantly less relative velocity between particle and fluid phases than indicated by the macroscopic relative velocity.

Possible effects of the new force terms in the macroscopic equations are examined from a one-dimensional simulation of a fluidized bed. Significant effects from the new terms on vertical pressure gradient and particle volume fraction distributions are observed. Published by Elsevier Science Ltd.

Keywords: Mesoscale structures; Averaged equations; Fluidized bed; Added mass; Drag reduction

1. Introduction

It is now well known that in many two-phase flows, such as in a fluidized bed, particle distributions are not uniform, but rather quite inhomogeneous (Schnitzlein and Weinstein, 1988). Clusters, streamers and bubbles exist in the flow (Grace and Tuot, 1979; Tsuji et al., 1998; Tsuo

* Corresponding author.
E-mail address: dzhang@lanl.gov (D.Z. Zhang).

0301-9322/02/$ - see front matter Published by Elsevier Science Ltd.
PII: S0301-9322(02)00005-8

and Gidaspow, 1990; Gidaspow, 1994). Recent numerical solutions using averaged equations for gas–solid two-phase flows performed by Sundaresan (2000) with fine grid resolution shows the important effects of these mesoscale structures. It is shown that for a practical fluidized bed, numerical simulations which ignore these mesoscale effects can be grossly inaccurate. This suggests that the traditional two-phase flow averaged equation model cannot be used directly to simulate these flows in typical practical engineering devices without using excessively fine grids. On the other hand, some recent studies suggest that, when fine enough grid resolution is used, the classical two-phase flow averaged equations do capture key features of two-phase flows with reasonable quantitative accuracy. For example, Zhang and VanderHeyden (2001) simulated a small fluidized bed using a set of highly simplified two-phase flow equations. Reasonable agreement between the numerical results and experimental data was observed with high resolution. Similar conclusions are also reached by Pan et al. (2000) in simulating bubbly flows. Comparison of their numerical results with several sets of experimental data demonstrates that simple physical models can capture key features of bubbly flows with high resolution.

The fact that the highly simplified two-phase flow model can produce reasonable numerical predictions using high grid resolution implies that the effects of mesoscale structures can be as—or even more—important than phase interactions at the particle scale. Indeed, Agrawal (2000) reported that the contribution to effective stress from particle-scale interactions as modeled by kinetic theory is negligible compared to the contributions from mesoscale interactions. Thus a theoretical framework for two-phase flows which includes the effects of mesoscale structures is essential for developing tools useful for practical engineering calculations.

One may attempt to derive an averaging framework which incorporates only a single average over both particle-scale and mesoscale fluctuations. Although this is a logically valid approach, to achieve this, the closure models constructed for this framework have to be able to describe physics for both particle-scale and mesoscale phenomena. Such closure models are practically difficult to obtain given that there are no generally accepted conceptual models for phase interactions that apply to both the particle and the mesoscale.

An alternative framework employs a two-average approach wherein equations are first derived from an average over the particle scale and then further averaged over the mesoscale. Given the fact that mesoscale structures are usually large compared to particle size, a scale separation between the mesoscale interactions and particle scale interactions can be assumed and exploited. Thus the two-step average framework has the advantage of conceptually splitting a difficult multiscale closure modeling task into two sets of relatively easier ones involving separately the particle scale and the mesoscale. In addition to the conceptual advantages, the two-average approach has a very practical advantage due to the success of the studies of Zhang and VanderHeyden (2001) and Pan et al. (2000). As mentioned above these researchers showed that equations from a first average which only incorporate particle-scale closure models can be used to compute two-phase flows in agreement with experiment as long as mesoscale phenomena are resolved by the calculations. This, then, provides the macroscopic flow closure modeler with intricate and complete numerical data sets from these high-resolution first-average simulations very much like the direct numerical simulation data sets being used by single-phase turbulence modelers. It is then very natural and self-consistent for the modeler using these data sets to then average the first-average equations used in these high-resolution simulations to produce macroscopic two-phase flow equations. This is the approach adopted in this paper.

The starting point for our analysis is to use the first-average equations (with only particle-scale closure) obtained by Zhang and Prosperetti (1994, 1997) using an ensemble phase-average technique. In this paper, we apply a second average using the Zhang–Prosperetti averaging technique to the first-average equations. As we shall see, application of the second average reveals new terms which are important to the modeling the macroscopic behavior of two-phase flows. The properties of the new closure terms are then studied using the numerical results from highly resolved three-dimensional simulations from Zhang and VanderHeyden (2001).

The concept of performing a second average is not new. If we take the point view of Irving and Kirkwood (1950) the Navier–Stokes equations are the averaged equations derived from a statistical theory of molecular systems. Thus, the Navier–Stokes equations correspond to our averaged equations obtained from the first average. The Reynolds averaged equations for turbulent flow then would correspond to our second average in this paper. Similarly, for fluidized beds, Dasgupta et al. (1994, 1997) performed a time average over a set of volume-averaged equations for two-phase flows. Also, the second average method was applied by Besnard and Harlow (1988) to examine the Reynolds stresses and energy cascade processes in turbulent two-phase flows. In present paper, instead of investigating the behavior of Reynolds stress, we examine the correlation between pressure gradient fluctuations and the fluctuations of the volume fraction.

2. Average over mesoscale

The averaged equations for two-phase flows have been derived by many researchers using various averaging methods, such as the volume average (Anderson and Jackson, 1967), the time average (Ishii, 1975), and the ensemble average (Batchelor, 1970; Drew, 1983). In this paper, we shall use the ensemble phase average technique introduced by Zhang and Prosperetti (1994, 1997). The tools developed in the ensemble phase average are extended to perform the second average over the averaged equations for two-phase flows. One of the advantages of following the ensemble phase average method introduced by Zhang and Prosperetti is that many of resulting closure terms from the second average correspond to terms in the averaged equation obtained from the first average; the relation between them will help us understand the physics associated with the new terms introduced by the second average.

In absence of phase change, the averaged continuity equation for the continuous phase is

$$\frac{\partial \theta_c \rho_c}{\partial t} + \nabla \cdot (\theta_c \rho_c \mathbf{u}_c) = 0, \tag{1}$$

and for the disperse phase is

$$\frac{\partial \theta_d \rho_d}{\partial t} + \nabla \cdot (\theta_d \rho_d \mathbf{u}_d) = 0, \tag{2}$$

where subscripts c and d are for the continuous phase and the disperse phase, respectively. The volume fraction for each phase is denoted by θ, the density by ρ and the averaged velocity by $\mathbf{u}$.

The momentum equations are

$$\frac{\partial}{\partial t}(\theta_c \rho_c \mathbf{u}_c) + \nabla \cdot (\theta_c \rho_c \mathbf{u}_c \mathbf{u}_c) = \theta_c \nabla \cdot \boldsymbol{\sigma}_c + \nabla \cdot (\theta_d \mathbf{L} + \theta_c \rho_c \mathbf{M}_c) - \theta_d \mathbf{f} + \theta_c \rho_c \mathbf{g}, \tag{3}$$

$$\frac{\partial}{\partial t}(\theta_{\mathrm{d}}\rho_{\mathrm{d}}\mathbf{u}_{\mathrm{d}}) + \nabla\cdot(\theta_{\mathrm{d}}\rho_{\mathrm{d}}\mathbf{u}_{\mathrm{d}}\mathbf{u}_{\mathrm{d}}) = \theta_{\mathrm{d}}\nabla\cdot\boldsymbol{\sigma}_{\mathrm{c}} + \nabla\cdot[\theta_{\mathrm{d}}(\rho_{\mathrm{d}}\mathbf{M}_{\mathrm{d}} + \boldsymbol{\sigma}_{\mathrm{coll}})] + \theta_{\mathrm{d}}\mathbf{f} + \theta_{\mathrm{d}}\rho_{\mathrm{d}}\mathbf{g}, \tag{4}$$

where is $\boldsymbol{\sigma}_{\mathrm{c}}$ is the averaged stress in the continuous phase. The quantity $\mathbf{L}$ can be proved (Prosperetti and Zhang, 1996) to be essentially the difference between averaged disperse phase stress $\boldsymbol{\sigma}_{\mathrm{d}}$ and the averaged continuous phase stress $\boldsymbol{\sigma}_{\mathrm{c}}$, which results from phase interactions at the microscopic level. The quantity $\mathbf{f}$ is the phase interaction force. The quantities $\mathbf{M}_{\mathrm{c}}$ and $\mathbf{M}_{\mathrm{d}}$ are the kinematic Reynolds stresses in the continuous and disperse phases resulting from fluctuations at the particle scale. The quantity $\boldsymbol{\sigma}_{\mathrm{coll}}$ is the stress due to collision among particles in the flow. The term $\mathbf{g}$ is the body force, such as the gravity. In the case of binary collisions $\boldsymbol{\sigma}_{\mathrm{coll}}$, is often modeled by kinetic theory disregarding effects of interstitial fluid. In the case of multi-particle collisions in the presence of an interstitial fluid, Zhang and Rauenzahn (1997, 2000) proved that the dynamics effect of interaction forces among particles can also be represented by a stress. In the case of a dilute potential flow, $\mathbf{f}$ is the added-mass and $\mathbf{L}$ is related to the relative velocity between the two phases (Zhang and Prosperetti, 1994). In a dilute Stokes flow, $\mathbf{f}$ is the Stokes drag and $\mathbf{L}$ is related to the effective viscosity of the suspension (Zhang and Prosperetti, 1997). The purpose of this paper, however, is not to examine these closure terms, but to study the effect of the mesoscale terms found in the equations from the second average.

To achieve this, we now perform a second average to derive macroscopic equations. Let $\mathscr{C}$ be a set of parameters uniquely determining the two-phase flow, and $P(\mathscr{C},t)$ be the probability density associated with $\mathscr{C}$ at time t. The second ensemble average of a quantity f is defined as

$$\overline{f}(\mathbf{x},t) = \int f(\mathbf{x},\mathscr{C},t)P(\mathscr{C},t)\,\mathrm{d}\mathscr{C}. \tag{5}$$

For a quantity f of phase i (i = c or d), the second ensemble phase average is defined as

$$\langle f\rangle_i(\mathbf{x},t) = \frac{\overline{\theta_i(\mathbf{x},t)f(\mathbf{x},t)}}{\overline{\theta}_i}. \tag{6}$$

Application of the average (5) to both sides of continuity Eqs. (1) and (2) leads to

$$\frac{\partial\overline{\theta}_{\mathrm{c}}\rho_{\mathrm{c}}}{\partial t} + \nabla\cdot(\rho_{\mathrm{c}}\overline{\theta}_{\mathrm{c}}\langle\mathbf{u}_{\mathrm{c}}\rangle_{\mathrm{c}}) = 0, \tag{7}$$

$$\frac{\partial\overline{\theta}_{\mathrm{d}}\rho_{\mathrm{d}}}{\partial t} + \nabla\cdot(\rho_{\mathrm{d}}\overline{\theta}_{\mathrm{d}}\langle\mathbf{u}_{\mathrm{d}}\rangle_{\mathrm{d}}) = 0. \tag{8}$$

For simplicity, in this paper we assume that both of the phases are incompressible. Similarly, averaging over the momentum equation for the disperse phase and adding and subtracting $\overline{\theta}_{\mathrm{d}}\nabla\cdot\langle\boldsymbol{\sigma}_{\mathrm{c}}\rangle_{\mathrm{c}}$, to the right-hand side, one finds

$$\rho_{\mathrm{d}}\left[\frac{\partial\overline{\theta}_{\mathrm{d}}\langle\mathbf{u}_{\mathrm{d}}\rangle_{\mathrm{d}}}{\partial t} + \nabla\cdot(\overline{\theta}_{\mathrm{d}}\langle\mathbf{u}_{\mathrm{d}}\rangle_{\mathrm{d}}\langle\mathbf{u}_{\mathrm{d}}\rangle_{\mathrm{d}})\right] = \overline{\theta}_{\mathrm{d}}\nabla\cdot\langle\boldsymbol{\sigma}_{\mathrm{c}}\rangle_{\mathrm{c}} + \nabla\cdot[\overline{\theta}_{\mathrm{d}}(\rho_{\mathrm{d}}\langle\mathbf{M}_{\mathrm{d}}\rangle_{\mathrm{d}} + \rho_{\mathrm{d}}\mathbf{M}_{\mathrm{dm}} + \langle\boldsymbol{\sigma}_{\mathrm{coll}}\rangle_{\mathrm{d}})] + \overline{\theta}_{\mathrm{d}}\langle\mathbf{f}\rangle_{\mathrm{d}} + \overline{\theta}_{\mathrm{d}}\mathbf{f}_{\sigma} + \overline{\theta}_{\mathrm{d}}\rho_{\mathrm{d}}\mathbf{g}, \tag{9}$$

where

$$\overline{\theta}_{\mathrm{d}}\mathbf{f}_{\sigma} = \overline{\theta_{\mathrm{d}}\nabla\cdot(\boldsymbol{\sigma}_{\mathrm{c}} - \langle\boldsymbol{\sigma}_{\mathrm{c}}\rangle_{\mathrm{c}})} = \overline{\theta}_{\mathrm{d}}\langle\nabla\cdot(\boldsymbol{\sigma}_{\mathrm{c}} - \langle\boldsymbol{\sigma}_{\mathrm{c}}\rangle_{\mathrm{c}})\rangle_{\mathrm{d}}, \tag{10}$$

and $\mathbf{M}_{\rm dm}$ is the kinematic Reynolds stress resulting from the second average

$$\mathbf{M}_{\rm dm} = -\langle(\mathbf{u}_{\rm d} - \langle\mathbf{u}_{\rm d}\rangle_{\rm d})(\mathbf{u}_{\rm d} - \langle\mathbf{u}_{\rm d}\rangle_{\rm d})\rangle_{\rm d}. \tag{11}$$

The appearance of the Reynolds stress $\rho_{\rm d}\overline{\theta}_{\rm d}\mathbf{M}_{\rm dm}$ is not unexpected. However, the appearance of the force term $\mathbf{f}_\sigma$ is less familiar. We shall examine this new force.

Similar to (9) one can write the momentum equation for the continuous phase as

$$\rho_{\rm c}\left[\frac{\partial\overline{\theta}_{\rm c}\langle\mathbf{u}_{\rm c}\rangle_{\rm c}}{\partial t} + \nabla\cdot\left(\overline{\theta}_{\rm c}\langle\mathbf{u}_{\rm c}\rangle_{\rm c}\langle\mathbf{u}_{\rm c}\rangle_{\rm c}\right)\right] = \overline{\theta}_{\rm c}\nabla\cdot\langle\boldsymbol{\sigma}_{\rm c}\rangle_{\rm c} + \overline{\theta_{\rm c}\nabla\cdot\left(\boldsymbol{\sigma}_{\rm c} - \langle\boldsymbol{\sigma}_{\rm c}\rangle_{\rm c}\right)} + \nabla\cdot\left(\overline{\theta}_{\rm d}\langle\mathbf{L}\rangle_{\rm d} + \overline{\theta}_{\rm c}\rho_{\rm c}\mathbf{M}_{\rm c}\right) + \nabla\cdot\left(\overline{\theta}_{\rm c}\rho_{\rm c}\mathbf{M}_{\rm cm}\right) - \overline{\theta}_{\rm d}\langle\mathbf{f}\rangle_{\rm d} + \overline{\theta}_{\rm c}\rho_{\rm c}\mathbf{g}, \tag{12}$$

where $\mathbf{M}_{\rm cm}$ is the kinematic Reynolds stress resulting from the second average

$$\mathbf{M}_{\rm cm} = -\langle(\mathbf{u}_{\rm c} - \langle\mathbf{u}_{\rm c}\rangle_{\rm c})(\mathbf{u}_{\rm c} - \langle\mathbf{u}_{\rm c}\rangle_{\rm c})\rangle_{\rm c}. \tag{13}$$

The second term on the right-hand side of (12) is similar to the mesoscale interfacial force $\overline{\theta}_{\rm d}\mathbf{f}_\sigma$ defined in (10). The volume fraction in this term is $\theta_{\rm c}$ instead of $\theta_{\rm d}$ as in (10). We now show that the difference of these two terms is a divergence of a stress. First note that

$$\overline{\theta_{\rm c}\nabla\cdot(\boldsymbol{\sigma}_{\rm c} - \langle\boldsymbol{\sigma}_{\rm c}\rangle_{\rm c})} = \overline{(\boldsymbol{\sigma}_{\rm c} - \langle\boldsymbol{\sigma}_{\rm c}\rangle_{\rm c})\cdot\nabla\theta_{\rm d}} = \nabla\cdot(\bar{\theta}_{\rm d}\mathbf{L}_{\rm m}) - \bar{\theta}_{\rm d}\mathbf{f}_\sigma, \tag{14}$$

where the first identity comes from differentiation by parts and definition (6) which yields $\overline{\theta_{\rm c}(\sigma_{\rm c} - \langle\sigma_{\rm c}\rangle_{\rm c})} = 0$, The second identity comes from definition (10) and by defining

$$\mathbf{L}_{\rm m} = \langle\boldsymbol{\sigma}_{\rm c}\rangle_{\rm d} - \langle\boldsymbol{\sigma}_{\rm c}\rangle_{\rm c}. \tag{15}$$

This quantity is similar to $\mathbf{L}$ which is essentially the averaged stress difference inside and outside particles (Prosperetti and Zhang, 1996). The quantity $\mathbf{L}_{\rm m}$, now, can be said to be the averaged stress difference inside and outside clusters or other mesoscale structures.

The momentum equation can now be written as

$$\rho_{\rm c}\left[\frac{\partial\overline{\theta}_{\rm c}\langle\mathbf{u}_{\rm c}\rangle_{\rm c}}{\partial t} + \nabla\cdot\left(\overline{\theta}_{\rm c}\langle\mathbf{u}_{\rm c}\rangle_{\rm c}\langle\mathbf{u}_{\rm c}\rangle_{\rm c}\right)\right] = \overline{\theta}_{\rm c}\nabla\cdot\langle\boldsymbol{\sigma}_{\rm c}\rangle_{\rm c} + \nabla\cdot\left[\bar{\theta}_{\rm d}(\langle\mathbf{L}\rangle_{\rm d} + \mathbf{L}_{\rm m}) + \bar{\theta}_{\rm c}\rho_{\rm c}\left(\langle\mathbf{M}_{\rm c}\rangle_{\rm c} + \mathbf{M}_{\rm cm}\right)\right] - \bar{\theta}_{\rm d}\langle\mathbf{f}\rangle_{\rm d} - \bar{\theta}_{\rm d}\mathbf{f}_\sigma + \bar{\theta}_{\rm d}\rho_{\rm c}\mathbf{g}. \tag{16}$$

Similar to the situation for the interfacial force discussed above, the macroscopic momentum equations for both phases contain the Reynolds stresses which have two parts, the microscopic part and mesoscopic part.

In the averaged momentum Eqs. (9) and (16), the stress $\langle\boldsymbol{\sigma}_{\rm c}\rangle_{\rm c}$ is the averaged stress weighted by volume fraction $\theta_{\rm c}$ of the continuous phases as defined in (6). Although this is a well-defined quantity, it will often be more useful to work both experimentally and theoretically in terms of the averaged stress of the mixture,

$$\langle\boldsymbol{\sigma}_{\rm c}\rangle_{\rm m} = \bar{\theta}_{\rm d}\langle\boldsymbol{\sigma}_{\rm c}\rangle_{\rm d} + \bar{\theta}_{\rm c}\langle\boldsymbol{\sigma}_{\rm c}\rangle_{\rm c} = \langle\boldsymbol{\sigma}_{\rm c}\rangle_{\rm c} + \bar{\theta}_{\rm d}\mathbf{L}_{\rm m}. \tag{17}$$

For this purpose, using (17) we can rewrite the momentum equations as

$$\rho_{\mathrm{d}}\left[\frac{\partial\bar{\theta}_{\mathrm{d}}\langle\mathbf{u}_{\mathrm{d}}\rangle_{\mathrm{d}}}{\partial t}+\nabla\cdot\left(\bar{\theta}_{\mathrm{d}}\langle\mathbf{u}_{\mathrm{d}}\rangle_{\mathrm{d}}\langle\mathbf{u}_{\mathrm{d}}\rangle_{\mathrm{d}}\right)\right]=\bar{\theta}_{\mathrm{d}}\nabla\cdot\langle\boldsymbol{\sigma}_{\mathrm{c}}\rangle_{\mathrm{m}}+\nabla\cdot\left[\bar{\theta}_{\mathrm{d}}\left(\rho_{\mathrm{d}}\langle\mathbf{M}_{\mathrm{d}}\rangle_{\mathrm{d}}+\rho_{\mathrm{d}}\mathbf{M}_{\mathrm{dm}}+\langle\boldsymbol{\sigma}_{\mathrm{coll}}\rangle_{\mathrm{d}}\right)\right]+\bar{\theta}_{\mathrm{d}}\langle\mathbf{f}\rangle_{\mathrm{d}}+\bar{\theta}_{\mathrm{d}}\mathbf{f}_{\mathrm{m}}+\overline{\theta}_{\mathrm{d}}\rho_{\mathrm{d}}\mathbf{g},\tag{18}$$

$$\rho_{\mathrm{c}}\left[\frac{\partial\bar{\theta}_{\mathrm{c}}\langle\mathbf{u}_{\mathrm{c}}\rangle_{\mathrm{c}}}{\partial t}+\nabla\cdot\left(\bar{\theta}_{\mathrm{c}}\langle\mathbf{u}_{\mathrm{c}}\rangle_{\mathrm{c}}\langle\mathbf{u}_{\mathrm{c}}\rangle_{\mathrm{c}}\right)\right]=\bar{\theta}_{\mathrm{c}}\nabla\cdot\langle\boldsymbol{\sigma}_{\mathrm{c}}\rangle_{\mathrm{m}}+\nabla\cdot\left[\bar{\theta}_{\mathrm{d}}\langle\mathbf{L}\rangle_{\mathrm{d}}+\bar{\theta}_{\mathrm{c}}\rho_{\mathrm{c}}\left(\langle\mathbf{M}_{\mathrm{c}}\rangle_{\mathrm{c}}+\mathbf{M}_{\mathrm{cm}}\right)\right]-\bar{\theta}_{\mathrm{d}}\langle\mathbf{f}\rangle_{\mathrm{d}}-\bar{\theta}_{\mathrm{d}}\mathbf{f}_{\mathrm{m}}+\bar{\theta}_{\mathrm{c}}\rho_{\mathrm{c}}\mathbf{g},\tag{19}$$

where

$$\bar{\theta}_{\mathrm{d}}\mathbf{f}_{\mathrm{m}}=\bar{\theta}_{\mathrm{d}}\mathbf{f}_{\sigma}-\bar{\theta}_{\mathrm{d}}\nabla\cdot(\bar{\theta}_{\mathrm{d}}\mathbf{L}_{\mathrm{m}})=\overline{\theta'_{\mathrm{d}}\nabla\cdot(\boldsymbol{\sigma}_{\mathrm{c}}-\langle\boldsymbol{\sigma}_{\mathrm{c}}\rangle_{\mathrm{m}})}.\tag{20}$$

The second identity of (20) comes from the definitions (10), (15) and the identity $\overline{\theta_{\mathrm{c}}\left(\boldsymbol{\sigma}_{\mathrm{c}}-\langle\boldsymbol{\sigma}_{\mathrm{c}}\rangle_{\mathrm{c}}\right)}=0$.

The force $\mathbf{f}_{\mathrm{m}}$ appears in the momentum equations for both phases with opposite sign. It is thus an exchange force. From its definition (20), it is clear that this force is the result of inhomogeneous distributions of particle volume fraction and stress divergence. To understand the physical meaning of the term $\mathbf{f}_{\mathrm{m}}$, let us consider an idealized bubble in a fluidized bed. Inside the bubble, the particle volume fraction is zero and outside the bubble particle volume fraction is a constant $\bar{\theta}_{\mathrm{d}}$. With this idealization we have a constant $\theta'_{\mathrm{d}}=-\bar{\theta}_{\mathrm{d}}$. Let V_{b} be the volume of the bubble, S be the surface of the bubble and $\mathbf{n}$ be the normal of the surface. The volume integral

$$\int_{V_{\mathrm{b}}}\theta'_{\mathrm{d}}\nabla\cdot(\boldsymbol{\sigma}_{\mathrm{c}}-\langle\boldsymbol{\sigma}_{\mathrm{c}}\rangle_{\mathrm{m}})\,\mathrm{d}v=-\bar{\theta}_{\mathrm{d}}\int_{S}(\boldsymbol{\sigma}_{\mathrm{c}}-\langle\boldsymbol{\sigma}_{\mathrm{c}}\rangle_{\mathrm{m}})\cdot\mathbf{n}\,\mathrm{d}S\tag{21}$$

is the interfacial force acting on the bubble excluding the effect of mean stress divergence. Similar to a single bubble in a pure fluid, the force $\mathbf{f}_{\mathrm{m}}$ represents the averaged interfacial force on the bubble such as, for example, the averaged added-mass force, the drag and Basset history force. Indeed, the interfacial force $\mathbf{f}_{\mathrm{d}}$ is defined similarly to Eq. (20) and is found to be the particle added-mass force and particle drag (Zhang and Prosperetti 1994, 1996). In many cases of practical interest, the Basset forces are negligible. For this reason, we shall not discuss this force further in this paper. The difference between force $\mathbf{f}_{\mathrm{d}}$ and $\mathbf{f}_{\mathrm{m}}$ is that they represent interactions at different length scales. The force $\mathbf{f}_{\mathrm{d}}$ represents particle-fluid interaction at the particle length scale, while the force $\mathbf{f}_{\mathrm{m}}$ represents interactions at the mesoscale. With this we can identify this force $\mathbf{f}_{\mathrm{m}}$ as the added-mass force and drag of mesoscale structures. In the case of gas–solid fluidized beds, interactions at the mesoscopic length scale are dominated by inertia of the flow (Davidson, 1961; Davidson et al., 1977). The drag component of $\mathbf{f}_{\mathrm{m}}$ is dominated, for example, by form drag. Added-mass of particles is usually negligible since the gas density is small compared to the density of the solid particles; added-mass of mesoscale structures is not negligible since the "fluid" surrounding these structures in a fluidized bed is not a pure gas, but rather is a mixture of gas and particles with density of the order of the mixture density, $\theta_{\mathrm{c}}\rho_{\mathrm{c}}+\theta_{\mathrm{d}}\rho_{\mathrm{d}}$, which is usually significantly larger than the gas density ρ_{c}. This is especially true in the case of "bubbles" in a gas–solid bed

wherein the dense "emulsion" surrounding bubble structures has a density of the order of the solid particles themselves. The added-mass component of the interfacial force, $\int_S (\boldsymbol{\sigma}_c - \langle \boldsymbol{\sigma}_c \rangle_m) \cdot \mathbf{n}\, dS$, can be written as $-C_b V_b \rho_e (\mathbf{a}_b - \mathbf{a}_e)$, where C_b is the added-mass coefficient for the bubble, ρ_e is the density of "emulsion" surrounding the bubble, $\mathbf{a}_b$ is the acceleration of the bubble and $\mathbf{a}_e$ is the acceleration of the "emulsion". In a bubbling gas–solid fluidized bed, if we neglect the drag component of the mesoscale force $\mathbf{f}_m$ and the interactions among bubbles, the added-mass force density can be written as

$$\bar{\theta}_d \mathbf{f}_m = -\bar{\theta}_d \theta_b C_b \rho_e (\mathbf{a}_e - \mathbf{a}_b), \tag{22}$$

where θ_b is the bubble volume fraction in the fluidized bed.

Although, the example provided above is an idealized case, it demonstrates the concept of mesoscale added-mass represented by the force term $\mathbf{f}_m$ defined by (20) in general two-phase flows with mesoscale structures.

Although considering interactions among mesoscale structures, such as interactions between bubbles and surrounding emulsion, resembles the idea of using the buoyancy based on mixture density in the momentum equation for two-phase flows, the appearance of the mesoscale force $\mathbf{f}_m$ is not a revival of the discussion among Clift et al. (1987), Fan et al. (1987), and Gibilaro et al. (1987) about the used of mixture pressure in a two-phase flow. It is important to note that, as defined in (20), the mesoscale force $\mathbf{f}_m$ results from the inhomogeneity in the distribution of volume fraction. The mesoscale force results from interactions at mesoscale level, and is not a force representing interactions between a particle and the mixture which happens at the particle scale.

In the next section we shall study the behavior of the closures terms, and then propose potential closures in Section 4.

3. Numerical simulations and results

To examine the behavior of closure quantities we use numerical data from our simulation (Zhang and VanderHeyden, 2001) of an experimental circulating fluidized bed (Van den Moortel et al., 1998). The averaged equations used in the simulation, are essentially the same equations used by Pan et al. (2000), which were obtained by Zhang and Prosperetti (1994, 1997) including the effects of particle-fluid drag and particle-scale added-mass only.

The geometry of the device used by Van den Moortel et al. had a 20 cm × 20 cm cross-section and was 200 cm in height. Particles in the experiment had mean diameter of 120 μm and a density of 2400 kg/m^3. In their experiments, the overall particle volume fraction was maintained at 3% using solids flow loop control. The experiments of Van den Moortel et al. correspond to the so-called "turbulent regime," (Grace, 1986). The turbulent regime, for so-called Group A powders, occurs for excess gas superficial velocities in the range of 0.5–2.0 m/s. Strictly speaking, the turbulent regime does not exhibit circulation like the so-called "fast fluidization regime". Thus, there appears to be some kind of discrepancy here. Nevertheless, Van den Moortel et al. do report circulation from their experiments. This apparent discrepancy can be resolved by considering the phenomena of particle entrainment from non-circulating fluid beds. As explained in Grace (1982), there is a zone above a fluid bed, whose height is called the "transport disengagement height" or

TDH, in which there can be significant particle entrainment. This zone is sometimes called the freeboard region. Using the graphic correlation provided by Zenz and Weil (1958), we can estimate the TDH to be about 3–4 m for the experiment of Van den Moortel, et al. for the case of a superficial gas velocity of 1.1 m/s. Since Van den Moortel's riser was only 2 m tall, we can presume that there was considerable particle entrainment from their turbulent-regime fluidized bed. This, then, would account for the observed circulation and resolve the apparent discrepancy mentioned above.

The grid resolution used in our simulations was 0.645 cm × 0.645 cm × 1.29 cm. To maintain a constant overall particle volume fraction as in the experiment, in our simulation at the beginning of each time step, the particle inflow at the bottom is set to be the same as the particle outflow from the top calculated at the end of previous time step. The simulations were carried to a statistically steady state and data were collected for a sufficiently long time to calculate the closure terms identified above. As the first step toward understanding these new closure terms from the second average, we examine one-dimensional closures. Consequently averages of the simulation data were performed across horizontal sections of the fluidized bed.

Since the equations used in the numerical simulation were most accurate for dilute situations, we only used the numerical simulation results from the computational cells in which the particle volume fraction was less than 20% when evaluating closure models. At bottom of the fluidized bed, particle pressure is used to prevent the particle volume fraction from going beyond the close packing limit. In addition, to avoid effects of the outflow boundary condition, we also excluded the data from the region close to the exit where the cross-section geometry was changed to emulate the experimental riser duct outlet (Zhang and VanderHeyden, 2001).

Mesoscale structures were observed in the simulation as illustrated in Fig. 1 and good agreement with experimental data was obtained as is shown in Fig. 2. As shown in Fig. 1, at the bottom of the fluidized bed, the distribution of particle volume fraction is nearly uniform because of the assumed uniform in-flow boundary conditions. Mesoscale structures are generated about 5 cm from the bottom. At a height of about 50 cm transition from turbulent fluidized bed to freeboard region occurs. Above this height, cluster–streamer type mesoscale structures are observed.

These flow transitions can be seen to correspond to the behavior of the mesoscale interaction force $\mathbf{f}_m$. The vertical component of this force computed from the simulation is plotted against height in Fig. 3. From the bottom of the column to a height of about 50 cm, the force diminishes from 0 to a minimum value of about -250 dN/cm^3, approximate location of the transition from turbulent fluidized bed to freeboard region. We hypothesize that this corresponds to the evolution of mesoscale structures from the bottom of the column. As we move up further, the force then grows becoming positive reaching a value of about 150 dN/cm^3 at a height of 160 cm. In the bottom of the column, the force acts to decelerate the particles. Since acceleration process are significant at the bottom of the column, we hypothesize that $\mathbf{f}_m$ is dominated by an mesoscale added-mass effect. The net effect is a retardation of the particle acceleration process. This will turn out to be one of the most important observations of this study. Towards the top of the column, the mesoscale force is positive and most likely is due to the drag on clusters–streamers like structures. At this end of the column, acceleration is diminished and so, therefore, is the added-mass component of the mesoscale interaction force.

With these hypothetical interpretations, we now proceed to explore some more quantitative models for the exchange force terms.

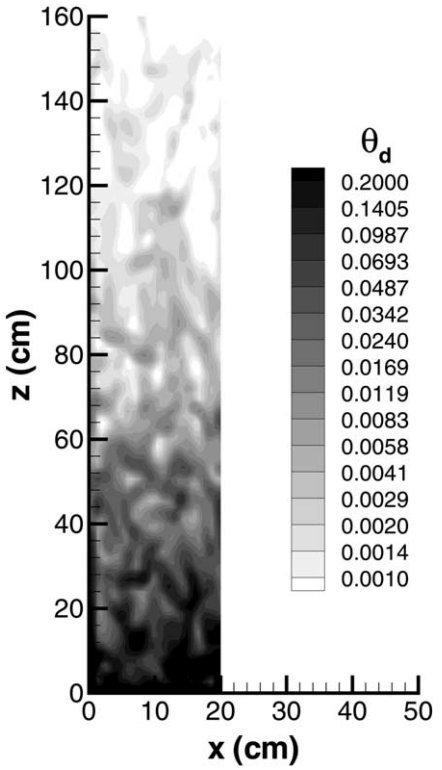

Fig. 1. Particle volume fraction contour on a mid-plane ($y = 10$ cm).

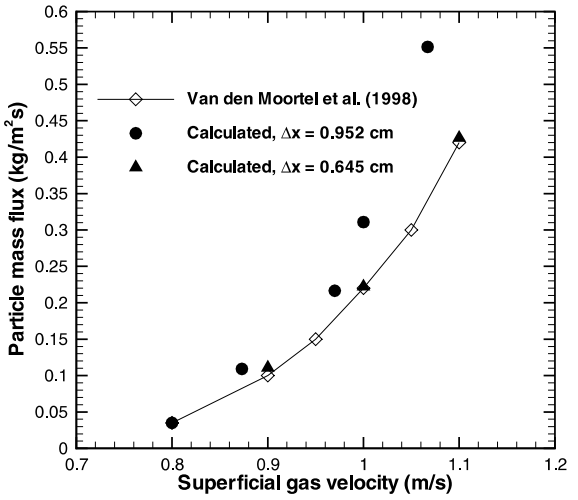

Fig. 2. Comparison between calculated particle mass fluxes and experimental results at different superficial gas velocities. The aspect ratio $\Delta x : \Delta y : \Delta z$ in these simulations is 1:1:2.

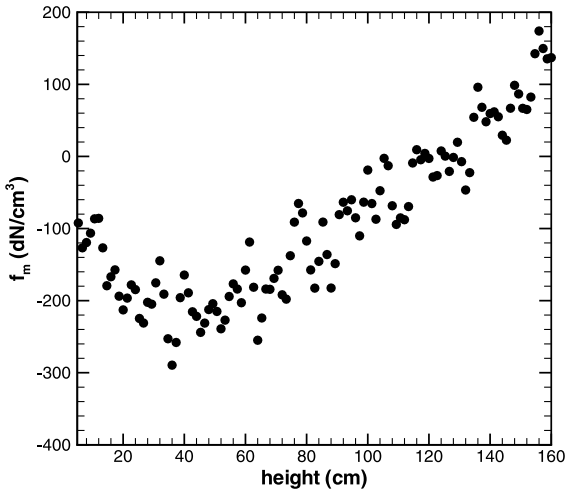

Fig. 3. Mesoscale force $\mathbf{f}_m$ as a function of height. The superficial gas velocity is 1.1 m/s.

4. Possible models for the closures

We focus here on the new interaction force terms $\mathbf{f}_m$ and $\langle \mathbf{f} \rangle_d$ obtained from the second average. Let us delay extensive discussion of potential closure models for the Reynolds stresses to future work and first consider the behavior of $\mathbf{f}_m$. As noted in previous sections, the force $\mathbf{f}_m$ can be expected to be composed of an added-mass force and a drag force associated with mesoscale structures. Also, as mentioned before, the force $\mathbf{f}_m$ at lower elevations has a negative vertical component which acts to resist the upward acceleration of particles. The force $\mathbf{f}_m$ is in the same direction of the relative velocity, $\langle \mathbf{u}_d \rangle_d - \langle \mathbf{u}_c \rangle_c$; therefore the force shown in Fig. 3 cannot be attributed to drag alone. In fact, as mentioned above, it appears to be dominated by an added-mass force component. At higher elevation, about 120 cm above the distributor, the vertical component of the force $\mathbf{f}_m$ becomes positive. At this point, the mesoscale drag appears to dominate over the added-mass force to resist the falling of clusters–streamer like structures as shown in Fig. 1. In the case of fluidized beds, the bottom portion has a higher particle volume fraction, and the added-mass component of the mesoscale force $\mathbf{f}_m$ is apparently more important than the drag component. At the end of Section 2, we demonstrated that the added-mass component of $\bar{\theta}_d \mathbf{f}_m$ can be expressed in terms of relative acceleration between the mesoscale structure (bubble in the example) and the surrounding emulsion. Since quantities associated with bubble or emulsion are not primary variables in the macroscopic equations, to have a closure relation for force $\mathbf{f}_m$ we need to relate the relative acceleration $\mathbf{a}_e - \mathbf{a}_b$ to the relative acceleration between the disperse phase and the continuous phase $\mathbf{a}_d - \mathbf{a}_c$. In a bubbling bed, we assume that the relative acceleration $\mathbf{a}_d - \mathbf{a}_c$ is caused by the interaction of bubbles and the surrounding emulsion and write

$$\mathbf{a}_d - \mathbf{a}_c = C_f \theta_b \bar{\theta}_d (\mathbf{a}_e - \mathbf{a}_b), \tag{23}$$

where C_f is an O(1) proportionality coefficient, θ_b is the bubble volume fraction. The quantity $\bar{\theta}_d$ is present because it represents the coupling between the disperse phase and the emulsion. Using (22), the added-mass component of $\bar{\theta}_d \mathbf{f}_m$ can be written as

$$\bar{\theta}_{\mathrm{d}}\mathbf{f}_{\mathrm{m}} = -C_{\mathrm{a}}\rho_{\mathrm{m}}(\mathbf{a}_{\mathrm{d}} - \mathbf{a}_{\mathrm{c}}), \quad \text{where } C_{\mathrm{a}} = \frac{C_{\mathrm{b}}\rho_{\mathrm{e}}}{C_{\mathrm{f}}\rho_{\mathrm{m}}}, \tag{24}$$

and $\rho_{\mathrm{m}} = \bar{\theta}_{\mathrm{d}}\rho_{\mathrm{d}} + \bar{\theta}_{\mathrm{c}}\rho_{\mathrm{c}}$ is density of the mixture in the fluidized bed. We call C_{a} the generalized added-mass coefficient. Added-mass coefficient for an inclusion in a fluid is usually of O(1) (0.5 for a sphere). However the generalized added-mass coefficient C_{a} need not to be so. The emulsion density ρ_{e} outside a bubble can be significantly higher than the averaged mixture density ρ_{m}, therefore, the generalized added-mass coefficient can be well above unity. Although, Eq. (24) is obtained for bubbling fluidized beds, the basic physics outlined here applies to more general cases. In general the boundary of a mesoscale structure is not be well defined, and bubbles and emulsions can be realistically thought of as particle lean and rich regions. For this reason, (if the drag component of $\bar{\theta}_{\mathrm{d}}\mathbf{f}_{\mathrm{m}}$ can be neglected), we propose to model the added-mass component of $\bar{\theta}_{\mathrm{d}}\mathbf{f}_{\mathrm{m}}$ simply as

$$\bar{\theta}_{\mathrm{d}}\mathbf{f}_{\mathrm{m}} = -C_{\mathrm{a}}\rho_{\mathrm{m}}\left(\frac{\partial\langle\mathbf{u}_{\mathrm{d}}\rangle_{\mathrm{d}}}{\partial t} + \langle\mathbf{u}_{\mathrm{d}}\rangle_{\mathrm{d}}\cdot\nabla\langle\mathbf{u}_{\mathrm{d}}\rangle_{\mathrm{d}} - \frac{\partial\langle\mathbf{u}_{\mathrm{c}}\rangle_{\mathrm{c}}}{\partial t} - \langle\mathbf{u}_{\mathrm{c}}\rangle_{\mathrm{c}}\cdot\nabla\langle\mathbf{u}_{\mathrm{c}}\rangle_{\mathrm{c}}\right). \tag{25}$$

Ideally, the density used above should be the averaged density of the effective medium outside the discrete mesoscale structures. To avoid the introduction, at this point, of a closure relation for such a density, we assume it can be expressed proportional to the local average mixture density, viz. $C_{\theta}\rho_{\mathrm{m}}$. The coefficient of proportionality is then lumped in to the generalized added-mass coefficient C_{a} as in (24). As mentioned above, this generalized added-mass coefficient can be large compare to one. Using our numerical results from the lower portion (height less than 60 cm) of the fluidized bed, we calculated the added-mass coefficient C_{a} for the case of superficial gas velocity $\bar{\theta}_{\mathrm{c}}\langle\mathbf{u}_{\mathrm{c}}\rangle = 1.1$ m/s. The results are shown in Fig. 4. In the figure, the added-mass coefficient is seen to increase with height, corresponding to the development of mesoscale structures. In general the coefficient is expected to depend on the evolution of the mesoscale structures and therefore

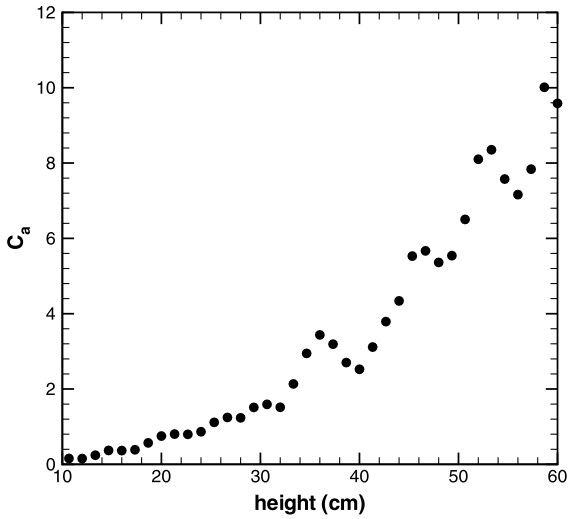

Fig. 4. Added-mass coefficient. The superficial gas velocity is 1.1 m/s.

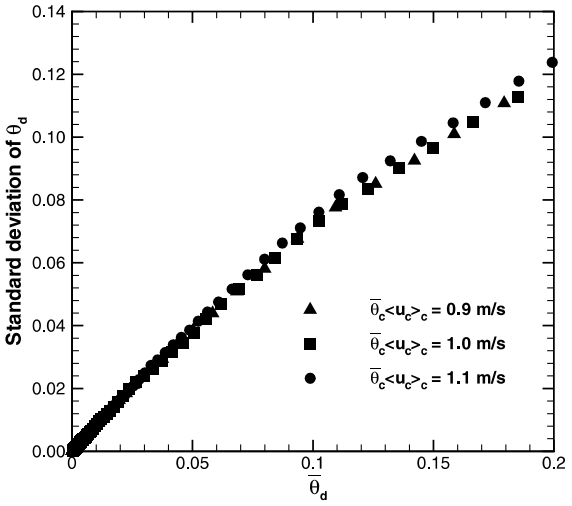

Fig. 5. Relation between standard deviation $\sqrt{\overline{\theta_{\mathrm{d}}'^2}}$ and $\bar{\theta}_{\mathrm{d}}$.

should depend on the geometry and the local solid and gas velocities. This makes a general model for the added-mass coefficient quite complicated and further research is clearly needed here.

In the upper region of the fluidized bed, the averaged particle volume fraction $\bar{\theta}_{\mathrm{d}}$ is small. According to Fig. 5 the fluctuation θ'_{d} and the stress difference $\boldsymbol{\sigma}_{\mathrm{c}} - \langle\boldsymbol{\sigma}_{\mathrm{c}}\rangle_{\mathrm{m}}$ are small too. From definition (20), it is easy to see that the force $\mathbf{f}_{\mathrm{m}}$ is also small and is less important than the added-mass in lower portion of the fluidized bed. Furthermore, the drag component of $\mathbf{f}_{\mathrm{m}}$ is much smaller that that due to particle-scale drag so we can, for practical purposes, model $\mathbf{f}_{\mathrm{m}}$ as, simply, an added-mass term given by Eq. (25).

Although the mesoscale force $\mathbf{f}_{\mathrm{m}}$ is often small compared to the particle-scale drag force, it does make a significant contribution to the momentum exchange in the fluidized bed where acceleration is important. To see this, we eliminate the stress divergence $\nabla\langle\boldsymbol{\sigma}_{\mathrm{c}}\rangle_{\mathrm{m}}$ from the momentum Eqs. (18) and (19) and then use (25) to find

$$\begin{aligned}
&\rho_{\mathrm{d}}\left[1 + C_{\mathrm{a}}\left(1 + \frac{\bar{\theta}_{\mathrm{c}}\rho_{\mathrm{c}}}{\bar{\theta}_{\mathrm{d}}\rho_{\mathrm{d}}}\right)\right]\left(\frac{\partial\langle\mathbf{u}_{\mathrm{d}}\rangle_{\mathrm{d}}}{\partial t} + \langle\mathbf{u}_{\mathrm{d}}\rangle_{\mathrm{d}}\cdot\nabla\langle\mathbf{u}_{\mathrm{d}}\rangle_{\mathrm{d}}\right) - \left[C_{\mathrm{a}}\rho_{\mathrm{d}} + \left(1 + \frac{C_{\mathrm{a}}\bar{\theta}_{\mathrm{c}}}{\bar{\theta}_{\mathrm{d}}}\right)\rho_{\mathrm{c}}\right] \\
&\quad\times\left(\frac{\partial\langle\mathbf{u}_{\mathrm{c}}\rangle_{\mathrm{c}}}{\partial t} + \langle\mathbf{u}_{\mathrm{c}}\rangle_{\mathrm{c}}\cdot\nabla\langle\mathbf{u}_{\mathrm{d}}\rangle_{\mathrm{c}}\right) \\
&= \frac{1}{\bar{\theta}_{\mathrm{d}}}\nabla\cdot\left[\bar{\theta}_{\mathrm{d}}\left(\rho_{\mathrm{d}}\langle\mathbf{M}_{\mathrm{d}}\rangle_{\mathrm{d}} + \rho_{\mathrm{d}}\mathbf{M}_{\mathrm{dm}} + \langle\boldsymbol{\sigma}_{\mathrm{coll}}\rangle_{\mathrm{d}}\right)\right] - \frac{1}{\bar{\theta}_{\mathrm{c}}}\nabla\cdot\left[\bar{\theta}_{\mathrm{d}}\langle\mathbf{L}\rangle_{\mathrm{d}} + \bar{\theta}_{\mathrm{c}}\rho_{\mathrm{c}}\left(\langle\mathbf{M}_{\mathrm{c}}\rangle_{\mathrm{c}} + \mathbf{M}_{\mathrm{cm}}\right)\right] \\
&\quad + \frac{1}{\bar{\theta}_{\mathrm{c}}}\langle\mathbf{f}\rangle_{\mathrm{d}} + (\rho_{\mathrm{d}} - \rho_{\mathrm{c}})\mathbf{g}.
\end{aligned} \tag{26}$$

Now it is easy to see the effect of mesoscale added-mass in the fluidized bed. In the equation above, the acceleration of the continuous phase is multiplied by $C_{\mathrm{a}}\rho_{\mathrm{d}} + (1 + (C_{\mathrm{a}}\bar{\theta}_{\mathrm{c}}/\bar{\theta}_{\mathrm{d}}))\rho_{\mathrm{c}}$, an effective density, which is significantly larger than ρ_{c} in the case of gas–solid flows. In the next

section we shall illustrate how the added-mass coefficient C_a affects the vertical profile of particle volume fraction.

Now let us consider the closure of the term $\langle \mathbf{f} \rangle_d$, the averaged particle-scale interaction force. The particle drag $\mathbf{f}_d$ is calculated in the simulations as a function of relative velocity between the two phases according to the classical expression for single-sphere drag.

$$\mathbf{f}_d = -\frac{3}{4d}\theta_c C_d \rho_g |\mathbf{u}_d - \mathbf{u}_c|(\mathbf{u}_d - \mathbf{u}_c). \tag{27}$$

The drag coefficient C_d, due to White (1974), is calculated as

$$C_d = C_\infty + \frac{24}{Re} + \frac{6}{1+\sqrt{Re}}, \quad Re = \frac{|\mathbf{u}_d - \mathbf{u}_c| d}{\nu_c}, \tag{28}$$

where ν_c is the kinematic viscosity of the continuous phase. In principle, the drag coefficient should also be modeled as a function of solids volume fraction to reflect the effect of particle-fluid-particle interactions. The well-known Richardson–Zaki model is an example. One of the purposes of this paper is to study interactions of mesoscale structures without relying on particle–particle interaction models, such as kinetic theory for granular flows. To be consistent, we elected to use the simple form for the drag and not to introduce effects of particle-fluid-particle interactions. As mentioned in our recently paper (Zhang and VanderHeyden, 2001), the error caused by neglecting these interactions is small since the particle volume fraction is low in the most of the fluidized bed under consideration. As stated in the last section, we only used the numerical data in the computational cells in which particle volume fraction was less than 20% when evaluating closure models. If a drag model accounting for the effects of particle concentration were used in the calculation, the drag would have been larger. As a consequence of this, the decrease of the particle volume concentration along the height of the bed would have been slower. However, the total solid flux would not have been changed significantly since the solid flux out of the fluidized bed was dominated by the upper region of the bed, where the particle concentration was low. Furthermore, we expect that the mesoscale structures observed would still be present.

One would hope that after the second average the averaged particle drag $\langle \mathbf{f} \rangle_d$ could be modeled as a function of the relative velocity $\langle \mathbf{u}_d \rangle_d - \langle \mathbf{u}_c \rangle_c$. But simply replacing relative velocity $\mathbf{u}_d - \mathbf{u}_d$ in Eqs. (27) and (28) above by $\langle \mathbf{u}_d \rangle_d - \langle \mathbf{u}_c \rangle_c$, significantly overpredicts the averaged particle drag $\langle \mathbf{f} \rangle_d$ as shown in Fig. 6. If, instead, one uses $\langle \mathbf{u}_d \rangle_d - \langle \mathbf{u}_c \rangle_d$, the results are very close to the value found from the numerical simulation. The physical explanation is that, on average, the continuous phase velocity "seen" by particles is $\langle \mathbf{u}_c \rangle_d$ instead of $\langle \mathbf{u}_c \rangle_c$. Unfortunately, the velocity $\langle \mathbf{u}_c \rangle_d$ is not a primary variable in the averaged equation system and has to be modeled. To better understand the averaged behavior of $\langle \mathbf{u}_c \rangle_d$ from our numerical results, let us define the relative velocity reduction coefficient C_r as

$$C_r = \frac{\langle u_{cz} \rangle_d - \langle u_{cz} \rangle_c}{\langle u_{dz} \rangle_d - \langle u_{cz} \rangle_c}, \tag{29}$$

where subscript z stands for vertical (z) direction. (This coefficient will have to be generalized for more complex, multi-dimensional situations. Nevertheless, we can learn a great deal from a one-dimensional analysis.) In the case of uniform θ_d, the difference between $\langle \mathbf{u}_c \rangle_d$ and $\langle \mathbf{u}_c \rangle_c$ vanishes and so does C_r. Therefore, the quantity C_r is a measure of inhomogeneity in the fluidized

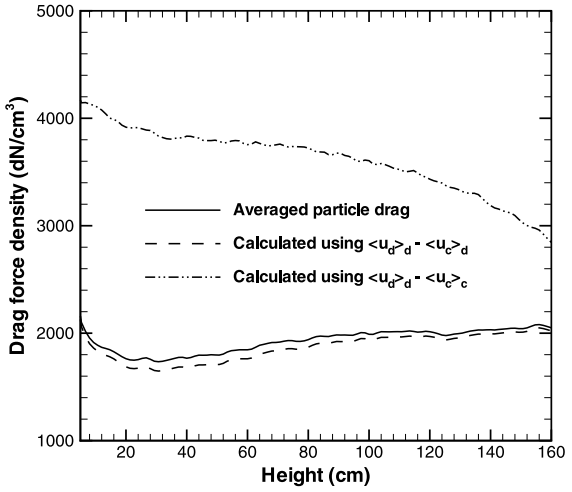

Fig. 6. Averaged particle drag force as a function of height. The solid line is results from numerical simulation and the dashed line is calculated using the gas velocity experienced by particles as in Eq. (31). The dot and dash line is calculated using averaged relative velocity $\langle \mathbf{u}_d \rangle_d - \langle \mathbf{u}_c \rangle_c$ as the relative velocity in (27). The superficial gas velocity is 1.1 m/s.

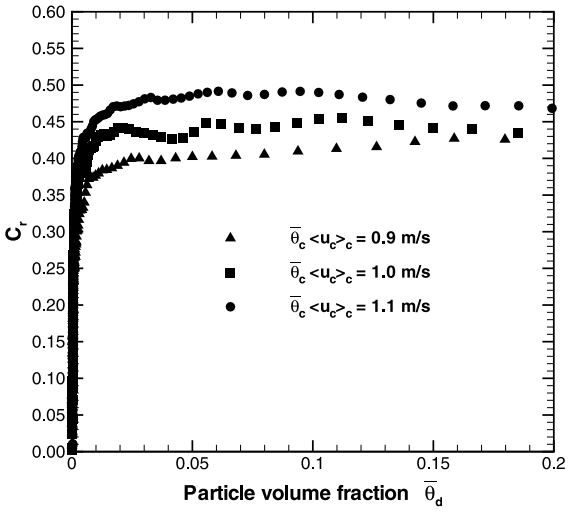

Fig. 7. Relative velocity reduction coefficient C_r.

bed. In Fig. 7, the quantity C_r is shown as a function of averaged particle volume fraction $\bar{\theta}_d$. The figure shows that at zero particle volume fraction, the value of C_r is zero since, in that case, the particle distribution is locally uniform. As can be seen, the value C_r increases rapidly over a very short range of $\bar{\theta}_d$ and then stays almost constant. We also note that the value of C_r should decrease to zero at the closed-packed volume fraction (0.6 in this case) since, in this limit, the distribution of the particle volume fraction θ_d must also be locally uniform. This effect, although not shown in the figure, was in fact observed in our numerical results.

With the above definition for C_r, the relative velocity felt by the particles is given

$$\langle u_{dz}\rangle_d - \langle u_{cz}\rangle_d = (1 - C_r)(\langle u_{dz}\rangle_d - \langle u_{cz}\rangle_c). \tag{30}$$

The averaged particle drag may then be modeled as

$$\langle \mathbf{f}\rangle_d = -\frac{3}{4d}\bar{\theta}_c C_d \rho_g (1 - C_r)^2 |\langle u_{dz}\rangle_d - \langle u_{cz}\rangle_c| (\langle u_{dz}\rangle_d - \langle u_{cz}\rangle_c), \tag{31}$$

where the drag coefficient C_d is calculated using the Reynolds number based on the averaged relative velocity $(1 - C_r)(\langle u_{dz}\rangle_d - \langle u_{cz}\rangle_c)$. The drag calculated using (31) is plotted in Fig. 6. Close agreement between this model and the simulation results is seen in the figure.

As a cautionary note, the authors would like to remind readers, that the closures proposed in this section are based on our numerical observations only. While we believe they are physically correct, they need to be tested and compared with experimental data since they are obtained from a fairly narrow range of conditions. We do expect, however, that they should extrapolate plausibly beyond our present dataset.

5. Effect of mesoscale structure on vertical profile of particle volume fraction

The device we simulated in previous section is rather small compared to typical devices in engineering practice. While the physics revealed in the study are expected to be valid in non-homogeneous fluidized beds, especially in gas–solid fluidized beds, the actual values of the coefficients are expected to vary in different situations since mesoscale structures are expected to depend, to some extent, on the boundary conditions and length scales of a given device. In this section, we examine the sensitivity of the coefficients introduced in the previous section. We also explore possible consequences of the mesoscale forces examined above in an industrial-scale device. We consider an example to see how the typically measured pressure gradient changes with the parameters C_a and C_r. In the example, the particle volume fraction is set at 0.33 at the inlet, the particle diameter is 75 μm, the solid flux is 135 kg/s/m^2, and the superficial velocity of gas is 5.20 m/s. The particle material density is 1700 kg/m^3 and gas is taken to be air at room temperature, with a density of 1.205 kg/m^3. These conditions are in the range appropriate for many industrial-scale fluidized beds. We consider a statistically steady one-dimensional fluidized bed. From the continuity Eqs. (7) and (8), we have

$$\bar{\theta}_c\langle u_c\rangle_c = Q_c, \quad \bar{\theta}_d\langle u_d\rangle_d = Q_d, \tag{32}$$

where Q_c and Q_d are superficial velocities of gas and solid. Given our asumptions, they are constants. Upon neglecting the Reynolds stresses, the collisional stresses $\langle \boldsymbol{\sigma}_{coll}\rangle$ and the stress $\langle \mathbf{L}\rangle_d$, Eq. (26) becomes

$$-\left\{\rho_d\left[1 + C_a\left(1 + \frac{\bar{\theta}_c\rho_c}{\bar{\theta}_d\rho_d}\right)\right]\frac{Q_d^2}{\bar{\theta}_d^3} + \left[C_a\rho_d + \left(1 + \frac{C_a\bar{\theta}_c}{\bar{\theta}_d}\right)\rho_c\right]\frac{Q_c^2}{\bar{\theta}_c^3}\right\}\frac{d\bar{\theta}_d}{dx}$$
$$= \frac{1}{\bar{\theta}_c}\langle \mathbf{f}\rangle_d + (\rho_d - \rho_c)\mathbf{g}. \tag{33}$$

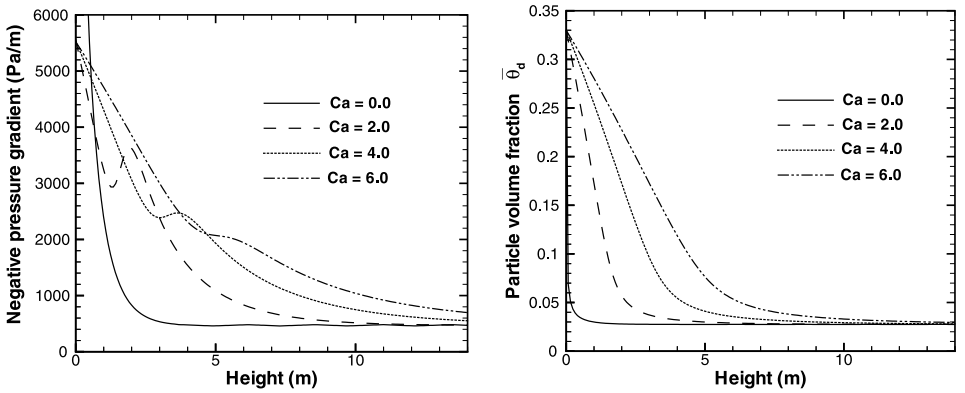

Fig. 8. Vertical distribution of pressure gradient and averaged partical volume fraction calculated using different added-mass coefficient C_a. The relative velocity reduction coefficient C_r is fixed at 0.9 in all calculations.

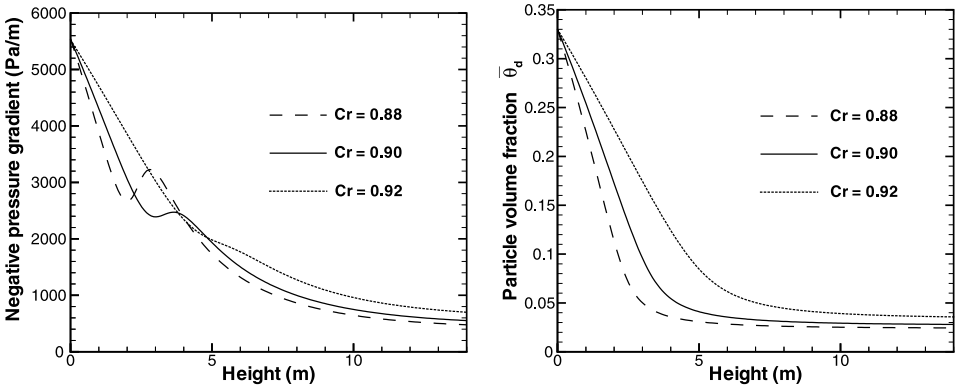

Fig. 9. Vertical distribution of pressure gradient and averaged partical volume fraction calculated using different relative velocity reduction coefficient C_r. The added-mass coefficient C_a is fixed at 4.0 in all calculations.

To illustrate the effects of the mesoscale added-mass and the drag reduction due to mesoscale structures, we examine solutions of (33) using constant values for the coefficients C_a and C_r. The drag is calculated using (31). Fig. 8 shows the effect of the added-mass coefficient on the pressure gradient and particle volume fraction distribution along the height of the fluidized bed. In the calculation, the coefficient C_r is set to 0.9. The effects of varying the value for C_r are shown on Fig. 9. Both figures show the qualitative importance of the effects of mesoscale added-mass and reduction of relative velocity due to mesoscale structures. Given this demonstration of the potential importance of these terms, more work should be performed to improve our understanding of these effects and in particular how mesoscale effects evolve from uniform conditions.

6. Conclusion

Based on numerical results obtained by high-resolution three-dimensional simulations of a circulating fluidized bed, it is found that the added-mass of mesoscale structures and drag re-

duction due to mesoscale structures are important. A set of macroscopic equations containing terms representing these mesoscale effects is obtained by extending the ensemble phase averaging method developed by Zhang and Prosperetti (1994, 1997) to include a second average.

Typically, the added-mass of particles in a gas–solid fluidized bed is negligible because of small gas density. However, the added-mass of mesoscale structures is important, since the density associated with the mesoscale added-mass is proportional to the mixture density instead of the density of the gas phase.

Also, inside a particle rich region, particles experience less relative velocity than indicated by the macroscopic relative velocity. Therefore, the averaged drag between the two phases is smaller than the drag calculated using the macroscopic averaged relative velocity. Possible closure models for the mesoscale added-mass and relative velocity reduction were introduced along with new coefficients C_a which characterizes the effective added-mass for mesoscale structures and C_r which characterizes relative velocity reduction.

Possible effects of the new mesoscale force terms in the macroscopic equations for two-phases flow are illustrated by computing the vertical profiles of pressure gradient and particle volume fraction in a fluidized bed using different values of the added-mass coefficient C_a and the relative velocity reduction coefficient C_r. The qualitative importance of these terms was demonstrated.

Acknowledgements

We gratefully acknowledge the support for this work by the US Department of Energy, Office of Industrial Technologies.

References

Agrawal, K., 2000. The role of mesoscale structures in rapid granular and gas–solid flows. Ph.D. Dissertation, Department of Chemical Engineering, Princeton University.

Anderson, T.B., Jackson, R., 1967. A fluid mechanical description of fluidized beds. Ind. Eng. Chem. Fundam. 6, 527–539.

Batchelor, G.K., 1970. The stress system in a suspension of force-free particles. J. Fluid Mech. 41, 545–570.

Besnard, D.C., Harlow, F.H., 1988. Turbulence in multiphase flow. Int. J. Multiphase Flow 14, 679–699.

Clift, R., Seville, J.P.K., Moore, S.C., Chavarie, C., 1987. Comments on buoyancy in fluidized beds. Chem. Eng. Sci. 42, 191–194.

Dasgupta, S., Jackson, R., Sundaresan, S., 1994. Turbulent gas-particle flow in vertical risers. AIChE J. 40 (2), 215–228.

Dasgupta, S., Jackson, R., Sundaresan, S., 1997. Developing flow of gas-particle mixture in vertical ducts. Ind. Eng. Chem. Res. 36, 3375–3390.

Davidson, J.F., 1961. Discussion. Trans. Instn. Chem. Engrs. 39, 230–232.

Davidson, J.F., Harrison, D., Guedes de Carvalho, J.R.F., 1977. On the liquid-like behavior of fluidized beds. Ann. Rev. Fluid Mech. 9, 55–86.

Drew, D.A., 1983. Mathematical modeling of two-phase flow. Ann. Rev. Fluid Mech. 15, 261–291.

Fan, L.-S., Han, L.S., Brodkey, R.S., 1987. Comments on the buoyancy force on a particle in a fluidized suspension. Chem. Eng. Sci. 42, 1269–1271.

Gibilaro, L.G., Di Felice, R., Waldram, S.P., Foscolo, P.O., 1987. Authors' reply to comments by Clift, et al.. Chem. Eng. Sci. 41, 194–196.

Gidaspow, D., 1994. Multiphase flow and fluidization. Academic Press, CA, pp. 31–58, 197–238.

Grace, J.R., 1982. Fluidized-bed hydrodynamics. In: Hetsroni, G. (Ed.), chapter 8 of Handbook of Multiphase Systems. Hemisphere, Washington.

Grace, J.R., 1986. Contacting modes and behavior classification of gas–solid and other two-phase suspensions. Can. J. Chem. Eng. 64, 353–363.

Grace, J.R., Tuot, J., 1979. A theory for cluster formation in vertically conveyed suspensions of intermediate density. Trans. Inst. Chem. Eng. 57, 49.

Irving, J.H., Kirkwood, I.G., 1950. The statistical mechanical theory of transport process. IV. The equations of hydrodynamics. J. Chem. Phys. 18, 817–829.

Ishii, M., 1975. Thermo-fluid dynamic theory of two-phase flow. Eyrolles, Paris.

Pan, Y., Dudukovic, M.P., Chang, M., 2000. Numerical investigation of gas-driven flow in 2-D bubble columns. AIChE J. 46, 434–449.

Prosperetti, A., Zhang, D.Z., 1996. Disperse phase stress in two-phase flow. Chem. Eng. Comm. 141–142, 387–398.

Schnitzlein, M.G., Weinstein, H., 1988. Flow characterization in high-velocity fluidized beds using pressure fluctuations. Chem. Eng. Sci. 43, 2605.

Sundaresan, S., 2000. Modeling the hydrodynamics of multiphase flow reactors: Current status and challenges. AIChE J. 46, 1102–1105.

Tsuji, Y., Tanaka, T., Yonemura, S., 1998. Cluster patterns in circulating fluidized beds predicted by numerical simulation (discrete particle model versus two-fluid model). Powder Technology 95, 254–264.

Tsuo, Y.P., Gidaspow, D., 1990. Computation of flow patterns in circulating fluidized beds. AIChE J. 36, 885–896.

Van den Moortel, T., Azario, E., Santini, R., Tadrist, L., 1998. Experimental analysis of the gas-particle flow in a circulating fluidized bed using a phase Doppler particle analyzer. Chem. Eng. Sci. 53, 1883–1899.

White, F.M., 1974. Viscous fluid flow. McGraw-Hill, New York.

Zenz, F.A., Weil, N.A., 1958. A theoretical-empirical approach to the mechanism of particle entrainment from fluidized beds. AIChE J. 4, 472–479.

Zhang, D.Z., Prosperetti, A., 1994. Averaged equations fro inviscid disperse two-phase flow. J. Fluid Mech. 267, 185–219.

Zhang, D.Z., Prosperetti, A., 1997. Momentum and energy equations for disperse two-phase flow and their closure for dilute suspensions. Int. J. Multiphase flow 23, 425–453.

Zhang, D.Z, Rauenzahn, R.M., 1997. A viscoelastic model for dense granular flow. J. Rheol. 41, 1275–1298.

Zhang, D.Z., Rauenzahn, R.M., 2000. Stress relaxation in dense and slow granular flows. J. Rheol. 45, 1019–1023.

Zhang, D.Z., VanderHeyden, W.B., 2001. High-resolution three-dimensional numerical simulation of a circulating fluidized bed. Powder Technology 116, 133–141.